# The relationship between the resonance frequency of a steering system and the tire-road friction coefficient

**Conference Paper** · September 2016

CITATIONS
0

READS
252

**5 authors**, including:

Long Chen
Tsinghua University
**18** PUBLICATIONS **56** CITATIONS
SEE PROFILE

Yugong Luo
Tsinghua University
**85** PUBLICATIONS **408** CITATIONS
SEE PROFILE

Zhaobo Qin
Tsinghua University
**15** PUBLICATIONS **32** CITATIONS
SEE PROFILE

Keqiang Li
Tsinghua University
**156** PUBLICATIONS **1,600** CITATIONS
SEE PROFILE

# The relationship between the resonance frequency of a steering system and the tire-road friction coefficient

L. Chen, Y. Luo, M. Bian, Z. Qin & K. Li
*State Key Laboratory of Automotive Safety and Energy, Tsinghua University, Beijing 100084, China*

ABSTRACT: Some researchers found the relationship between the resonance frequency of an in-wheel motor (IWM) drive system and the tire-road friction coefficient (TRFC), and used it to estimate TRFC. This paper tries to establish a similar relation between the road condition and the electric power steering system (EPS) frequency response, by analysing the dynamic characteristics. System modelling is conducted by coupling a lateral-relaxation-length based dynamic tire model and a simplified motor model. Then detailed analysis of the system dynamics in the frequency domain is provided by a deduced frequency response function, considering different system parameters, such as longitudinal velocity and the gear ratio. As a result of analysis, a function of the system resonance frequency (RF) which is related to TRFC is presented. Comparison of the RF is made between EPS and IWM to propose a TRFC estimation idea based on frequency domain data fusion. The correctness of the RF equation is demonstrated using a simulation model.

## 1 INTRODUCTION

Since the forces between the tires and road interface primarily determine the states of vehicle motion, the knowledge of tire-road friction coefficient (TRFC) can be extremely useful for many vehicle active safety control systems, including electric power steering (EPS), direct yaw torque control system (DYC), adaptive cruise control system (ACC) and unified chassis control, to get a better performance. Particularly, reliable estimation of friction coefficients at each wheel will enable both traction and stability control systems, reduce wheel skid and enhance driving stability. Many researches on vehicle stability control have also proposed the explicit use of tire-road friction information in determination of the desired yaw rate and other control system variable (Rajamani, R. 2005, Yanada, M. et al. 2005).

Abundant literatures illustrated the state of art of the estimation of tire-road friction coefficient, and several different approaches have been proposed, which can be classified into two categories: cause-based and effect-based.

Some researchers of cause-based method try to detect factors that affect the friction coefficient, using optical camera, ultrasonic sensor or other sensors to detect road coverings (such as ice, snow, etc.) so as to estimate the friction coefficient (Yanada, M. et al. 2005).

Effect-based methods directly focus on the vehicle motion effects generated by the determinate control input under certain tire-road friction condition. The effects were shown in the tire as acoustic characteristic, tire-tread deformation and wheel slip. Hong, S. et al. 2013 introduced a certain sensor that was fixed to the inner surface of the tire to observe tire deformation. However this method needed a specially equipped sensor and a signal transmitting apparatus. Gustafsson, F. 1997, and Lee, C. 2004 deemed that the slope between the slip ratio and friction coefficient curve could give the information. But as the longitudinal tire force can't be accurately estimated by using engine torque or braking pressure. Meanwhile, when driving the vehicle in a static situation, the slip ratio is small and sensitive to the noise of wheel speed signal. In a word, there are some limitations about the slope-based method just using time-domain information. Ono, E. et al. 2003 tried to estimate road condition using the frequency characteristic of wheel speed signals during braking (Umeno, T. et al. 2002). Bartram, M. et al. 2010 found the influence of the tyre/road contact interface on driveline vibrations.

While vehicle is traveling, the angular velocity of the wheel can be considered as two parts, namely the high-frequency and low-frequency signals. Slope-based estimation accuracy depends on the tire force and slip ratio, and each parameter can be influenced by the high-frequency signal and static deviation of the lower one. For high-frequency signal, unlike the

difficulty to accurately obtain the output torque of engine or braking pressure, in-wheel drive systems can control and capture the wheel driving torque in high frequency (Mutoh, N. 2012), which may bring a chance to estimate the friction coefficient using high frequency information of wheel speed. So unlike the normal traditional method using lower frequency information, Chen, L. et al. 2016 proposed to detect the difference of road condition based on a deduced relation between TRFC and the high motor-wheel resonance frequency. If this theory is also suitable for the lateral situation, a similar frequency relation should exist in the electric power steering system, and can be used to estimate TRFC.

In this paper, the dynamic characteristics of a steering system are focused on to estimate the tire-road friction coefficient. With a brief review of the traditional concept of lateral relaxation length and static tire model, a dynamic tire model for normal driving is introduced. After a PMSM mathematical model is studied, a transfer function from control signal of the motor to the steering column dynamics can be obtained. Then an insight into the steering system dynamics in the frequency domains is provided, through checking the impact of different parameters. As a result of these analysis, the paper obtains the equation of the system resonance frequency which is related to the tire-road friction. Comparison of the RF is given between EPS and IWM to propose a TRFC estimation idea based on frequency domain data fusion. A simulation model is applied to effectively reproduce the resonance phenomenon, and shows the correctness of this RF function.

The paper is organized as follows. In Section 2, a dynamic tire model and a mathematical model of the steering motor are established. Section 3 illustrates the deduction process of the frequency response function. The resonance phenomenon and the distinctive frequency are found in Section 4, observed in Section 5. Conclusions are given in the end.

## 2 SYSTEM MODELLING

### 2.1 *Electric power steering system*

Electric power steering system in this article is a column-assist-type, whose steering motor through the worm gear structure is connected to the steering column, steers front wheels by rotation of the steering column.

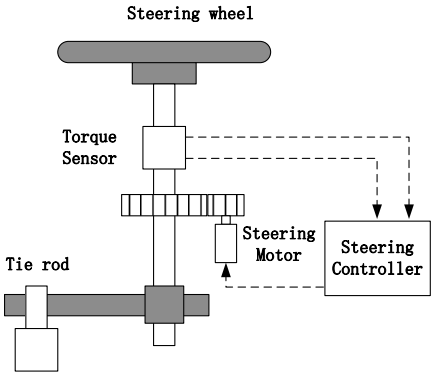


Figure 1. Schematic diagram of EPS (Ji-Hoon, K. et al. 2002)

Considering the torque balance of the the steering column, the system can be modelled as:

$$T_h + T_m G_m - \frac{T_a}{G_s} = B_d\dot{\theta}_d + J_d\ddot{\theta}_d \tag{1}$$

where, $T_h$ is the torque input of the driver, $T_m$ is the motor torque, $G_m$ is the worm gear ratio, $T_\alpha$ is the aligning torque of the front axle, $G_s$ is the gear ratio of the steering system form the steering wheel angle to the steering angle of the front wheel. $\theta_d$ is the steering angle of the column, $B_d$ is damping coefficient, $J_d$ is the equivalent moment of inertia.

### 2.2 *Tire model*

For the sake of simplicity, only lateral motion will be considered in this paper. The dynamics of suspension dynamics, road slope and so on are also neglected.

The tire system is then described as the following form.

$$\begin{aligned} T_\alpha^S &= k_\alpha \alpha \\ \alpha &= -\frac{\theta_d}{G_s} + \frac{v_y + l_f\omega_r}{v_x} \\ k_\alpha &= b\mu_{\max} + c \end{aligned} \tag{2}$$

where $T_\alpha^S$ is the steady aligning torque, $k_\alpha$ and $\alpha$ are the aligning stiffness and the sideslip angle of the front axle, respectively. $v_x$ and $v_y$ is the longitudinal and lateral velocity of the vehicle at the point of the centre of gravity(CoG), $\omega_r$ is the yaw rate of the vehicle around the vertical axis. $l_f$ is the distance from the front axle to CoG. $\mu_{\max}$ is the TRFC. $b$ and $c$ are two constants.

Some researchers show that the dynamic reaction of the tire force to disturbances can be approximated well using the first order systems. The non-linear relaxation length-based model is used to describe the dynamic aligning torque $T_\alpha^D$ derived from the steady aligning torque force $T_\alpha^S$ (Pacejka, H.B. 2002).

$$\tau\dot{T}_\alpha^D + T_\alpha^D = T_\alpha^S \tag{3}$$

The time constant $\tau$ can be derived from the relaxation length $r_y$ as follows:

$$\tau = \frac{r_y}{v_x} \tag{4}$$

In this study, to minimize the complexity of the calculation process, the non-linear characteristics of $r_y$ is ignored, and $r_y$ is set as a constant.

### 2.3 *I-PMSM model*

The following assumptions are made before establishing the mathematical model of I-PMSM:

1) Neglect the saturation of the electric motor ferrite core.

2) Neglect turbulent flow and hysteresis loss in the electric motor.

3) The currents in the electric motor are symmetrical three-phase sinusoidal currents.

4) d-axis inductance equals to q-axis inductance.

Hence, in this study, the motor model can be simplified as Equation (5) (Song, Z. et al. 2013):

$$T_m = Ki \tag{5}$$

where $K$ is a constant coefficient, $i$ is the current of the motor.

## 3 TRANSFER FUNCTION DEDUCTION

Assume that the motor torque includes two kinds of information, low frequency and high frequency, shown as follows.

$$T_m = T_0 + T_1 \sin(2\pi f \cdot t) \tag{6}$$

where $T_0$ is a constant value, standing for the low frequency information, while $T_1 \sin(2\pi f \cdot t)$ is the high frequency information, $T_1$ is the amplitude, $f$ means the frequency.

After substituting Equation (6) into Equation (1), the steering dynamic function can be described as Equation (7).

$$T_h + G_m\left(T_0 + T_1 \sin(2\pi f \cdot t)\right) - \frac{T_\alpha^D}{G_s} = B_d\ddot{\theta}_d + J_d\ddot{\theta}_d \tag{7}$$

With the derivative on both sides of Equation (7), Equation (8) will be obtained as

$$G_m(2\pi f)T_1 \cos(2\pi f \cdot t) - \frac{\dot{T}_\alpha^D}{G_s} = B_d\dddot{\theta}_d + J_d\ddot{\theta}_d \tag{8}$$

Then combine Equation (7) with (8) through multiplying Equation (8) by $\tau$ and adding up to Equation (7):

$$\begin{aligned} &T_h + G_m T_0 + G_m T_1\left[(2\pi f\tau)\cos(2\pi f \cdot t) + \sin(2\pi f \cdot t)\right] - \tau\frac{\dot{T}_\alpha^D}{G_s} - \frac{T_\alpha^D}{G_s} \\ &= B_d\ddot{\theta}_d + (\tau B_d + J_d)\dddot{\theta}_d + \tau J_d\ddot{\theta}_d \end{aligned} \tag{9}$$

Considering the dynamic and static tire model (Equation (2) and (3)), the equation above can be simplified as

$$\begin{aligned} &T_h + G_m T_0 + aG_m T_1 \sin(2\pi f \cdot t + \phi) - \frac{k_\alpha \alpha}{G_s} = B_d\ddot{\theta}_d + (\tau B_d + J_d)\dddot{\theta}_d + \tau J_d\ddot{\theta}_d \\ &a = \sqrt{1 + (2\pi f\tau)^2},\ \phi = \arctan(2\pi f\tau) \end{aligned} \tag{10}$$

Differentiating Equation (10) with respect to time, it can be expressed as:

$$\begin{aligned} &2\pi f a G_m T_1 \cos(2\pi f \cdot t + \phi) - \frac{k_\alpha \dot{\alpha}}{G_s} = B_d\dddot{\theta}_d + (\tau B_d + J_d)\ddot{\theta}_d + \tau J_d\dddot{\theta}_d \\ &\dot{\alpha} = -\frac{\dot{\theta}_d}{G} + \frac{\dot{v}_y + l_f\dot{\omega}_r}{v_x} \end{aligned} \tag{11}$$

In this paper, only the straight and moderate driving case is studied, which means that the longitudinal vehicle speed is approximately equal to the wheel rotation speed multiplied by effective rolling radius, and the steering angle of steering wheel is nearly zero. As the moment inertia of vehicle rather larger than the one of steering system, so the derivative of the rotation speed $\omega_r$ and the lateral velocity $v_y$ can be treated as zero, compared to the one of the steering angle. $\dot{v}_y + l_f\dot{\omega}_r \approx 0$ .Under these assumption, Equation (11) can be rewritten as:

$$2\pi f a G_m T_1 \cos(2\pi f \cdot t + \phi) = \frac{k_\alpha \dot{\theta}_d}{G_s^2} + B_d\ddot{\theta}_d + (\tau B_d + J_d)\dddot{\theta}_d + \tau J_d\ddot{\theta}_d \tag{12}$$

Assume:

$$T_2 = T_1 \cos(2\pi f \cdot t + \phi) \tag{13}$$

Equation (12) can be rearranged as:

$$2\pi f a G_m T_2 = \frac{k_\alpha \dot{\theta}_d}{G_s^2} + B_d\ddot{\theta}_d + (\tau B_d + J_d)\dddot{\theta}_d + \tau J_d\ddot{\theta}_d \tag{14}$$

Assume $\omega_d = \dot{\theta}_d$. With Laplace transform on both sides of Equation (14), it can be written as:

$$2\pi f a G_m T_2(\lambda) = \left[\frac{k_\alpha}{G_s^2} + B_d\lambda + (\tau B_d + J_d)\lambda^2 + \tau J_d\lambda^3\right]\omega_d(\lambda) \tag{15}$$

where, $\lambda$ is the Laplacian operator.

Then, ignoring the highest-order term $\tau J_d\lambda^3$ the transfer function from control signal of the motor to the steering column dynamics can be shown as:

$$\frac{T_2(\lambda)}{\omega_d(\lambda)} = \frac{\frac{k_\alpha}{G_s^2} + B_d\lambda + (\tau B_d + J_d)\lambda^2}{2\pi f a G_m} \tag{16}$$

But, in practical application, the current of the motor can be measured directly instead of the motor torque. So Equation (16) should be rearranged with Equation (5) as:

$$\frac{i(\lambda)}{\omega_d(\lambda)} = \frac{\frac{k_\alpha}{G_s^2} + B_d\lambda + (\tau B_d + J_d)\lambda^2}{2\pi f\sqrt{1 + (2\pi f\tau)^2}KG_m} \tag{17}$$

So the amplitude ratio between the current and the rotation speed is shown as:

$$\begin{aligned} \frac{A(i)}{A(\omega_d)} = \left|\frac{i(j2\pi f)}{\omega_d(j2\pi f)}\right| &= \frac{\left|\frac{k_\alpha}{G_s^2} - (\tau B_d + J_d)(2\pi f)^2 + jB_d(2\pi f)\right|}{2\pi f\sqrt{1 + (2\pi f\tau)^2}KG_m} \\ &= \frac{\left|\frac{k_\alpha}{G_s^2} - \left(\frac{B_d r_y}{v_x} + J_d\right)(2\pi f)^2 + jB_d(2\pi f)\right|}{2\pi f\sqrt{1 + \left(\frac{2\pi f r_y}{v_x}\right)^2}KG_m} \end{aligned} \tag{18}$$

## 4 RESONANCE FREQUENCY

With Equation (18), different impacts of system parameters on the steering column can be analysed.

### 4.1 *Effect of longitudinal velocity*

Figure 2 shows three amplitude ratio-frequency curves under different longitudinal velocities.

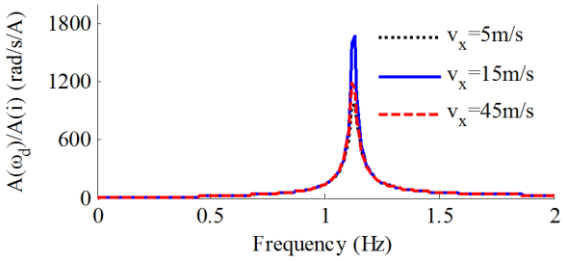


Figure 2. Amplitude ratio under different velocities*
*Parameters: $k_\alpha$ =2000Nm/rad; $r_y$ =0.05m; $G_s$ =20; $G_m$ =4; $K$ =6Nm/A; $B_d$ =0.03Nm-s/rad; $J_d$ =0.1 kg-m2.

This figure implies that, for most frequency range, the amplitude ratios are similar under different velocities, which means that longitudinal velocity shows little effect on the curve shape. When the frequency locates in the range 1.1-1.2 Hz, the curves reach separated peak points. Meanwhile, the peak value at 15 m/s is the highest among the three curve. It reflects that the velocity impact on the peak value is not linear, which should be considered in the control algorithm of EPS. The frequency of the peak point is called as steering system resonance frequency in this paper.

### 4.2 *Effect of gear ratio*

Figure 3 shows three amplitude ratio-frequency curves under different worm gear ratios.

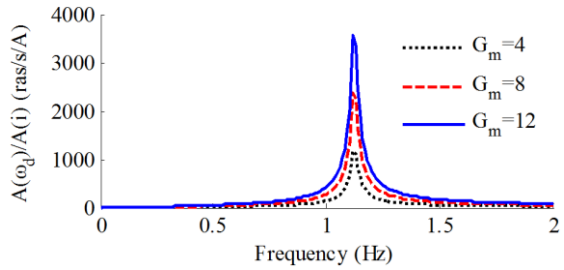


Figure 3. Amplitude ratio under different worm gear ratios *
*Parameters: $k_\alpha$ =2000Nm/rad; $r_y$ =0.05m; $G_s$ =20; $v_x$ =5m/s; $K$ =6Nm/A; $B_d$ =0.03Nm-s/rad; $J_d$ =0.1 kg-m2.

This figure implies that, steering system resonance frequency is not influenced by worm gear ratios. And the velocity impact on the curve shape is linear, which can easily be understood through Equation (18).

Figure 4 shows three amplitude ratio-frequency curves under different steering ratios.

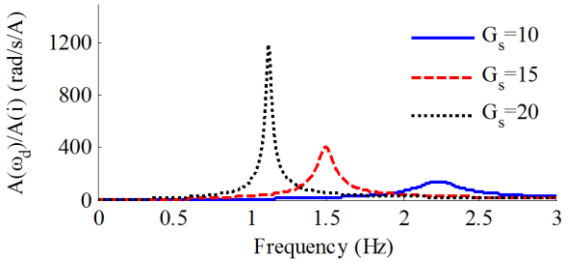


Figure 4. Amplitude ratio under different steering ratios *
*Parameters: $k_\alpha$ =2000Nm/rad; $r_y$ =0.05m; $G_m$ =4; $v_x$ =5m/s; $K$ =6Nm/A; $B_d$ =0.03Nm-s/rad; $J_d$ =0.1 kg-m2.

The steering ratio is an important parameter in the system design in order to reach a balanced optimization between manoeuvre ability and comfort. This figure clearly implies that, the smaller steering ratio is given, the low peak value and the higher system resonance frequency can be reached.

### 4.3 *Effect of aligning stiffness*

Figure 5 shows three amplitude ratio-frequency curves under different aligning stiffness.

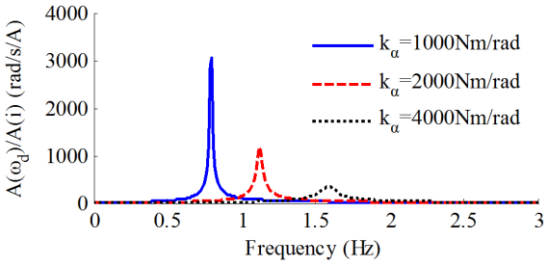


Figure 5. Amplitude ratio under different aligning stiffness*
*Parameters: $G_m$ =4; $r_y$ =0.05m; $G_s$ =20; $v_x$ =5m/s; $K$ =6Nm/A; $B_d$ =0.03Nm-s/rad; $J_d$ =0.1 kg-m2.

The aligning stiffness's impact shows the opposite trend to the one of the steering ratio. As this parameter can be influenced strongly by the vertical tire force and tire-road friction coefficient, its real-time estimation should be included in the EPS control algorithm.

### 4.4 *Steering system resonance frequency*

The resonance frequency cannot be obtained directly from Equation (17). From Figure 2-5, it shows that the empirical value of resonance frequency is smaller than 3 Hz.

With this empirical value, approximate conversion can be made on Equation (18).

$$\min\left[\frac{A(i)}{A(\omega_d)}\right] \approx \min\left[\frac{\left|\frac{k_\alpha}{G_s^2} - J_d(2\pi f)^2 + jB_d(2\pi f)\right|}{2\pi f K G_m}\right] = \min\left[\left|\frac{jB_d}{G_m} + \frac{\frac{k_\alpha}{G_s^2} - J_d(2\pi f)^2}{2\pi f K G_m}\right|\right] \quad (19)$$

After some mathematical deduction, the resonance frequency can be expressed as:

$$f_0 \approx \frac{1}{2\pi G_s}\sqrt{\frac{k_\alpha}{J_d}} = \frac{1}{2\pi G_s}\sqrt{\frac{b\mu_{\max}+c}{J_d}} \quad (20)$$

Apparently, Equation (20) explains the regular patterns discussed above and shown in Figure 2-5. As mentioned in the Introduction, Equation 20 shows the relationship between TRFC and the resonance frequency, which is similar to the motor-wheel resonance frequency function proposed in the reference (Chen, et al. 2016). Meanwhile, Using Equation 20, a TRFC estimation method which utilizes the high-frequency information of the motor current and steering column rotation speed can be investigated.

### 4.5 *RF Comparison between IWM and EPS*

As shown in Figure 5, the empirical value of the steering system resonance frequency is 1-3 Hz. Comparatively, the empirical value of the in-wheel motor drive system is 10 times of the former one, about 10-30 Hz, shown as Figure 6.

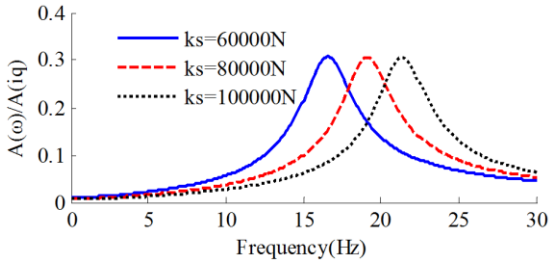


Figure 6. Resonance frequency of IWM* (Chen, et al. 2016)
* $k_s$ is the longitudinal stiffness, $\omega$ is the wheel speed, $i_q$ is the in-wheel motor current.

If the estimated TRFCs for each direction can be regarded as two measurements for the same signal subjected to different disturbances, they are significantly distinct from the viewpoint of frequency response and the model error. The estimated longitudinal TRFC can quickly response to the changing of road conditions, but the accuracy can be easily influenced by the model (the relation function between the IWM resonance frequency and the longitudinal TRFC) error and the "sensing error". In the research, "sensing error" refers to the error in the frequency domain, which actually means the noise or unstable and instantaneous vibration of the signal in the time domain. So, comparatively, even though the estimated lateral TRFC cannot quickly response to the changing of road conditions, it is relatively robust against the sensing instantaneous vibration and model errors.

## 5 SIMULATION OF RESONANCE FREQUENCY

A bicycle vehicle model which integrates the EPS and IWM is built to test the correctness of the resonance phenomenon. The main parameters of the vehicle model are listed in Table 1.

Table 1. The main parameters of the vehicle model

| Parameter | Values |
|---|---|
| Vehicle mass (kg) | 1274 |
| Wheel base (mm) | 2578 |
| Front and rear axle load ratio | 7:13 |
| Yaw inertia(kg-m2) | 1523 |
| $r_y$ (m) | 0.05 |
| $v_x$ (m/s) | 15 |
| $G_s$ (-) | 15.9 |
| $G_m$ (-) | 4 |
| $K$ (Nm/A) | 4 |
| $b$ (Nm/rad) | 5000 |
| $c$ (-) | 0 |
| $J_d$ (kg-m2) | 0.1 |
| $B_d$ (Nm-s/deg) | 0.03 |

In this simulation, the setting of the road surface is shown as Figure 7. With the given values of $G_s$, $J_d$, $b$, $c$, the steering system resonance frequency (RF) can be calculated using Equation 18. During 0-9 s, the RF is 2 Hz, and during 9-18 s, the RF is 1 Hz. The steering and driving motor torque demand is a kind of band-limited white noise around zero in order to keep a constant longitudinal velocity and go straight, shown as Figure 8.

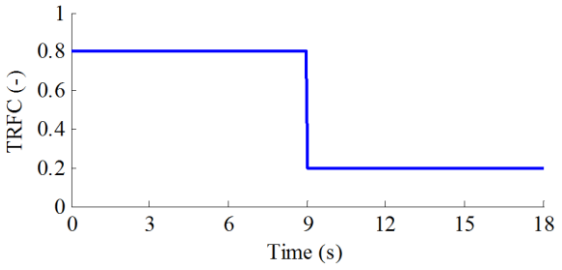


Figure 7. Setting of the TRFC

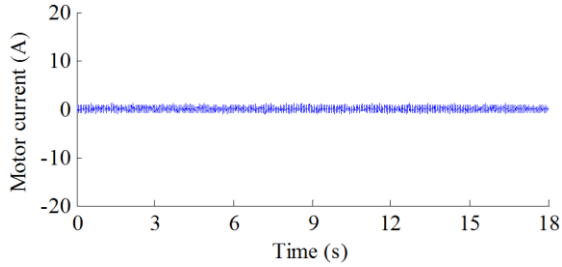


Figure 8. Current control input

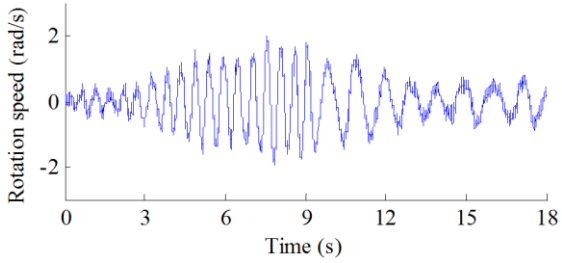


Figure 9. The steering wheel rotation speed

It can be seen clearly in Figure 9 that the oscillation cycle is respectively 0.5 s and 1 s before and after the time point of 9 s. This result coincides with the RF calculated in the last paragraph, and illustrates that the TRFC have a strong impact on the

steering system dynamic response and Equation 18 is reasonable.

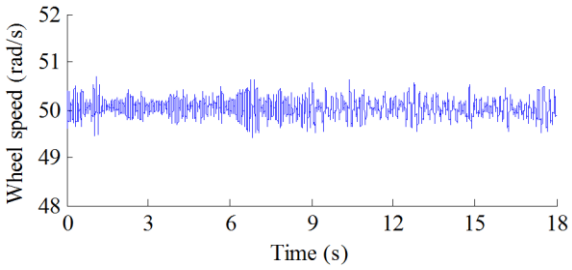

Figure 10. Wheel rotation speed without noise

The true value of wheel speed without noise was shown as Figure 10. It can be seen clearly that the signal before 9 s was more compressed than the one after 9 s. The oscillation cycle of the in-wheel motor system in Fig 10 was rather shorter than the one of the EPS in Figure 9, which verified the discussion in 'RF Comparison between IWM and EPS'.

So, in order to accurately capture the dynamic changing of road conditions, the higher-frequency information of the longitudinal TRFC estimation should be extracted. At low frequencies, the value from the lateral TRFC estimation is mainly used against model errors. To implement this idea, first order filters (Piyabongkarn, D. et al. 2009) are found to be adequate for the combination of the two directions' TRFC. The combination format is proposed as Equation (21).

$$\hat{\mu}_{\max} = \frac{1}{\tau_0 s + 1}\mu_{\max - y} + \frac{\tau_0 s}{\tau_0 s + 1}\mu_{\max - x} \tag{21}$$

where $\tau_0$ is a time constant, $\mu_{\max - y}$ is the estimated TRFC based on the steering RF, $\mu_{\max - x}$ is the one based on the IWM RF.

## 6 CONCLUSION

In this paper, a relationship between RF of a steering system and TRFC is observed by studying the dynamic characteristics. The insight into the system dynamics in the frequency domains is provided through a deduced system transfer function. The transfer function is be obtained by combining dynamic tire model with PMSM mathematical model. The relationship is verified by a simulation model.

Contributions of this paper:

- By introducing the notion of the lateral relaxation length, a transfer function of the dynamic steering system is obtained to explains the parameters impact in frequency domain;
- An equation of steering system resonance frequency is deduced, which is related to TRFC. As a future research direction, it can be used to propose an estimation method of the road condition without the information of the sideslip angle and aligning torque.
- Using frequency domain data fusion, the estimated combined TRFC can achieve quick response to the changing of road conditions in high frequency domain and stability to the signal noise in lower frequency domain.

## ACKNOWLEDGMENTS

The authors are grateful for the sponsorship from the the National Natural Science Foundation of China (Grant No. 51575295 and Grant No. U1564208).

## REFERENCES

Rajamani, R. 2005. *Vehicle Dynamics and Control*, New York.

Yanada, M. et al. 2005. Road surface condition detection technique based on image taken by camera attached to vehicle rearview mirror. *Review of Automotive Engineering*, 22: 163-168.

Hong, S. et al. 2013. Tyre–road friction coefficient estimation based on tyre sensors and lateral tyre deflection: modeling, simulations and experiments. *Vehicle System Dynamics*, 51(5): 627-647.

Gustaffson, F. 1997. Slip-based tire-road friction estimation. *Automatica*, 33(6): 1087–1099.

Lee, C. et al. 2004. Real-time slip-based estimation of maximum tire-road friction coefficient. *IEEE/ASME Transactions on Mechatronics*, 9(2): 454 – 458.

Umeno, T. et al. 2002. Estimation of tire-road friction using tire vibration model. *SAE Technical Papers*, 2002-01-1183.

Ono, E. et al. 2003. Estimation of automotive tire force characteristics using wheel velocity. *Control Engineering Practice*, 11: 1361-1370.

Bartram, M. et al. 2010. A study on the effect of road friction on driveline vibrations. *Proceedings of the Institution of Mechanical Engineers, Part K: Journal of Multi-body Dynamics*, 224: 321-340.

Mutoh, N. 2012. Front-and-rear-wheel-independent-drive type electric vehicle (FRID EV) with the outstanding driving performance suitable for next-generation electric vehicles. *2012 IEEE International Electric Vehicle Conference.*

Chen, L. et al. 2016. Tire–road friction coefficient estimation based on the resonance frequency of in-wheel motor drive system. *Vehicle System Dynamics*, 54(1):1-19.

Ji-Hoon, K. et al. 2002. Control logic for an electric power steering system using assist motor. *Mechatronics*, 12(3): 447-459.

Pacejka, H.B. 2002. *Tyre and vehicle dynamics*. Oxford: Butterworth-Heinemann.

Song, Z. et al. 2013. Rule-based fault diagnosis of hall sensors and fault-tolerant control of PMSM. *Chinese Journal of Mechanical Engineering*, 26(4): 813-822.

Piyabongkarn D, Rajamani R, Grogg J A, et al. 2009. Development and experimental evaluation of a slip angle estimator for vehicle stability control. *IEEE Transactions on Control Systems Technology*, 17(1): 78-88.